

Experimental quantum secure network with digital signatures and encryption

Hua-Lei Yin,^{1,*} Yao Fu,^{2,†} Chen-Long Li,^{1,2} Chen-Xun Weng,^{1,2} Bing-Hong Li,^{1,2} Jie Gu,¹ Yu-Shuo Lu,¹ Shan Huang,¹ and Zeng-Bing Chen^{1,2,‡}

¹National Laboratory of Solid State Microstructures, School of Physics, Collaborative Innovation Center of Advanced Microstructures, Nanjing University, Nanjing 210093, China
²MatricTime Digital Technology Co. Ltd., Nanjing 211899, China

Cryptography promises four information security objectives, namely, confidentiality, integrity, authenticity and non-repudiation, to support trillions of transactions every year in digital economy. While quantum key distribution together with one-time pad perfectly guarantees communication confidentiality, its counterpart of efficient digital signature, ensuring integrity, authenticity and non-repudiation of data, is highly wanted and an intractable open problem. Here we propose unconditionally secure quantum digital signatures consisting of secret sharing, one-time universal₂ hashing and one-time pad. The protocol promises to sign documents of up to 2^{64} lengths with security bound of 10^{-19} if only using 384-bit key. Furthermore, we build an all-in-one quantum secure network integrating provably secure communication, digital signatures, secret sharing and conference key agreement. Our work completes the toolbox of the four information security objectives.

Fast developing driverless, blockchain and artificial intelligence technology, as well as digital currency systems, will soon require a more robust network with security against quantum attacks [1]. A promising blueprint for such a network ensures one-way hash functions, encryption algorithms and digital signatures with information-theoretical security, which cannot be met in the current Internet with public-key infrastructure [2]. Currently, the widely implemented one-way hash functions, Message Digest-5 [3] and Secure Hash Algorithm-1 [4], are no longer secure. For example, one can utilize two different files to obtain the identical hash value after carrying out Secure Hash Algorithm-1 since 2017 [5]. Besides, the public-key (or asymmetric-key) encryption algorithms [6–8], based on the computational complexity of factorization [9] and discrete logarithm [10], both have been compromised at the 795-bit level in 2020 [8]. More seriously, quantum computer can in principle attack public-key cryptosystems with any number of bits [11].

Different from the public-key cryptography, one-time pad encryption based on a symmetric key provides a way of transmitting a message with provable confidentiality [12] over a standard communication channel, where the symmetric key is securely established using quantum key distribution [13] with no restriction on computational power of attackers. Currently, experimental demonstrations and commercial applications of quantum key distribution have arisen widely around the world [14–16].

The provable security brought out by quantum key distribution ensuring only confidentiality is, however, an incomplete solution to the remaining cryptographic tasks. In addition to confidentiality, three other fundamental information security objectives are data integrity, data origin authentication and non-repudiation [2], which are

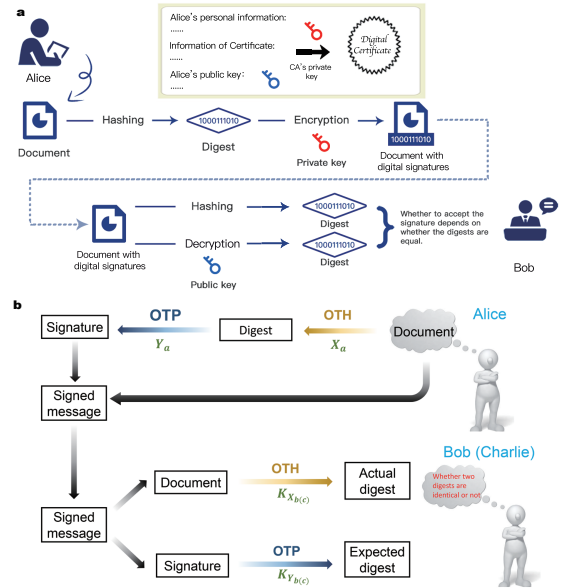


FIG. 1: **Schematic diagram for digital signatures.** **a**, Classical scheme with one-way hash function and public-key cryptography. Alice encrypts the digest to obtain the signature by private key, where the digest is acquired via a fixed one-way hash function. She sends the document along with the signature to Bob, who utilizes the same one-way hash function and the corresponding public key to acquire two digests, respectively. Then Bob accepts the signature if two digests are identical. Thereinto, digital certificate issued by certificate authority guarantees the validity of public key. **b**, Our QDS scheme with secret sharing, one-time universal₂ hashing (denoted as OTH) and one-time pad (OTP) encryption, where secret sharing can guarantee unconditional security via quantum laws. Compared with the classical scheme, Charlie plays the role of the certificate authority, Alice's key can be seen as private key while Bob's key is public key—they are asymmetric in our QDS protocol.

*Electronic address: hlyin@nju.edu.cn

†Electronic address: yaofu@mail.uustc.edu.cn

‡Electronic address: zbchen@nju.edu.cn

usually realized in classical cryptosystems by digital signatures using one-way hash functions and public-key en-

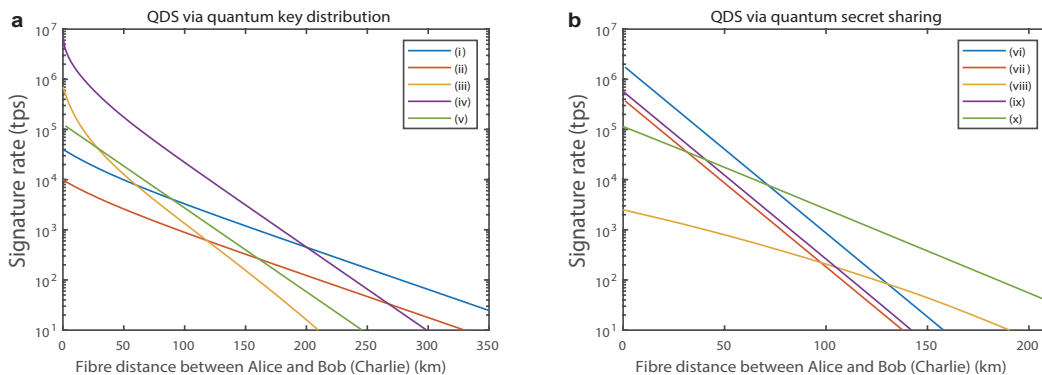


FIG. 2: **Signature rates versus fibre distances.** **a**, The rate via quantum key distribution. **b**, The rate via quantum secret sharing. Lines labelled (i)-(v) represent sending-or-not-sending twin-field (i), phase-matching (ii), discrete-modulated continuous-variable (iii), Gaussian-modulated continuous-variable (iv) and measurement-device-independent (v) quantum key distribution protocols. Lines labelled (vi)-(x) represent prepare-and-measure (vi), measurement-device-independent (vii), round-robin (viii), single-qubit (ix) and differential-phase-shift (x) quantum secret sharing protocols. To simplify, let the channel loss of Alice-Bob and Alice-Charlie be the same. We need 384-bit key for performing each digital signature with the security bound of about 1.1×10^{-19} for document of up to 2^{64} length. The signature rates are more than 10000 tps in the metropolitan area if we use a gigahertz system.

ryption algorithms, as shown in Fig. 1a. Digital signatures play a vital role in software distributions, e-mails, web browsing and financial transactions, but become insecure as one-way hash functions and public-key encryption algorithms used therein are breakable by either classical or quantum computers.

Different from classical solutions [9, 10], quantum digital signatures (QDS) promise to sign a document with provable integrity, authenticity and non-repudiation via quantum laws. The first rudiment of QDS was introduced in 2001 [17], but it could not be implemented due to some impractical requirements. Recent developments have removed the impractical requirements such as high-dimensional single-photon state [18], quantum memory [19] and secure quantum channels [20–22] and thus enable demonstrations of QDS in various experimental systems [23–28]. The resulting schemes still have serious limitation that requires about 10^5 -bit key to sign only one-bit message. The best signature rate reported so far is less than 1 time per second (tps) for one-bit message at 100 km transmission distance for a gigahertz system [27]. Additionally, one cannot know how to efficiently sign multi-bit messages with provable security, which makes all known QDS protocols impractical. Thus, QDS with both high efficiency and unconditional security is highly wanted and an intractable open problem.

Here we propose an entirely different QDS protocol capable of signing an arbitrarily long document with unconditional security. We simulate the performances of our QDS protocol based on varieties of quantum communication protocols. We also experimentally construct a trusted-repeater quantum secure network to realistically demonstrate the cryptographic primitives with information-theoretical security, including private communication, digital signatures, secret sharing and confer-

ence key agreement.

Our proposal utilizes secret sharing, one-time universal₂ hash function [29] and one-time pad encryption to generate and verify signatures (see Fig. 1B). Let Alice be the signer, Bob and Charlie be the receiver. Before executing the signing, all of them have two sets of keys, which satisfy the correlations $X_a = X_b \oplus X_c$ (n bits) and $Y_a = Y_b \oplus Y_c$ ($2n$ bits). Suppose that Alice signs an m -bit document (message), denoted as Mes , to the desired recipient, Bob. (i) Alice randomly generates an irreducible polynomial [30, 31] $p(x)$ of degree n , which can be characterized by an n -bit string p_a (see Supplemental Material). Then she uses her key bit string X_a and the irreducible polynomial $p(x)$ to generate a random linear feedback shift register-based (LFSR-based) Toeplitz matrix [32] H_{nm} with n rows and m columns. She acquires an $2n$ -bit digest $Dig = (Dig_1 || p_a)$. Thereinto, Dig_1 is the digest of the m -bit document through hash operation with $Dig_1 = H_{nm} \cdot Mes$ and p_a is an n -bit string for generating the irreducible polynomial in the LFSR-based Toeplitz matrix. Then Alice encrypts the digest with her key bit string Y_a to get the $2n$ -bit signature $Sig = Dig \oplus Y_a$. She sends the document and signature $\{Sig, Mes\}$ to Bob. (ii) Bob transmits $\{Sig, Mes\}$ as well as his key bit strings $\{X_b, Y_b\}$ to Charlie so as to inform Charlie that he has received the signature. Then Charlie forwards his key bit strings $\{X_c, Y_c\}$ to Bob. Bob obtains two new key bit strings $\{K_{X_b} = X_b \oplus X_c, K_{Y_b} = Y_b \oplus Y_c\}$ by XOR operation. He exploits K_{Y_b} to obtain an expected digest and a string p_b via XOR decryption. He utilizes K_{X_b} and p_b to establish an LFSR-based Toeplitz matrix and acquires an actual digest via hash operation. Bob will accept the signature if the actual digest is equal to the expected digest. Then he informs Charlie the result. (iii) If Bob announces that he accepts the signature, Charlie creates two new key bit

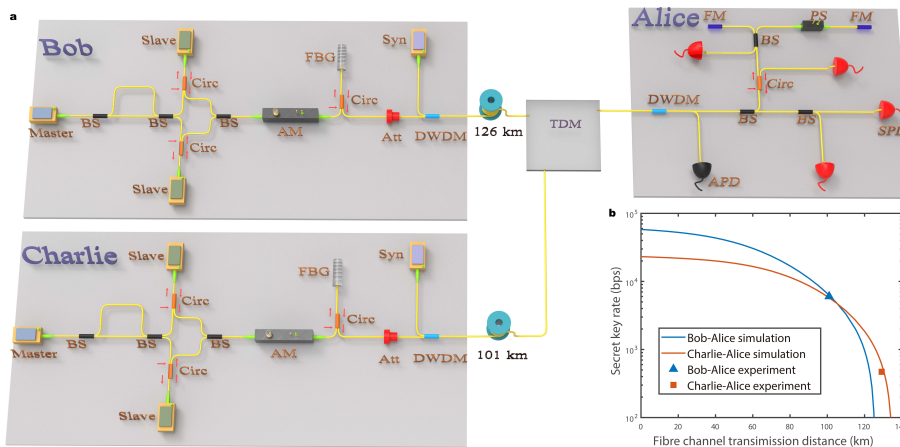


FIG. 3: **Experimental setup of the quantum secure network with quantum key distribution.** **a**, Bob (Charlie) exploits a master laser, an asymmetric interferometer, two slave lasers, two circulators (Circ) and a beam splitter (BS) to prepare optical pulses in the Z and X bases by controlling the trigger electrical signal of slave lasers. The decoy signals are generated by amplitude modulator (AM) while vacuum state is produced via removing the triggered signal of slave lasers. The optical pulses pass through a set of fiber Bragg grating (FBG), circulator and attenuator (Att) to be modulated at the single-photon level. The synchronization (Syn) signal is transmitted with dense wavelength division multiplexer (DWDM) to quantum channel. The synchronization pulse is detected by avalanche photodiode (APD). A biased beam splitter is utilized for realizing a passive basis measurement with single-photon detector (SPD). Two Faraday mirrors (FM), a phase shifter (PS) and a beam splitter form an asymmetric interferometer. The quantum signals sent by Bob (Charlie) arrive at Alice by time division multiplexing (TDM). **b**, Experiment results of decoy-state quantum key distribution. The blue and red curves of secret key rate correspond to simulation results using experiment parameters.

strings $\{K_{X_c} = X_b \oplus X_c, K_{Y_c} = Y_b \oplus Y_c\}$ using his original key and the key sent by Bob. He employs K_{Y_c} to acquire an expected digest and a variable p_c via XOR decryption. Charlie gets an actual digest via hash operation, where the hash function is a LFSR-based Toeplitz matrix generated by K_{X_c} and p_c . Charlie accepts the signature if the two digests are identical.

Note that if Alice, Bob and Charlie are all truthful, there is the relation $p_a = p_b = p_c$ and $X_a = K_{X_b} = K_{X_c}$. Thus, they will use the same universal₂ hash function and generate the same actual digest. The signature will be accepted naturally. One-time pad encryption [12] guarantees the digest with perfect privacy and hides all information about the Toeplitz hashing before Bob's decryption. One-time universal₂ hash function, specifically the LFSR-based Toeplitz matrix [32], ensures that the used hash function is completely random each time. In this way, Bob's probability of finding any two different documents with the same hash value is $m/(2^{n-1})$, which is practically an ignorable probability. An authenticated classical channel [32, 33] between Bob and Charlie, implemented by LFSR-based Toeplitz hashing and one-time pad encryption, is used to make sure that the corresponding new key bit strings of Bob and Charlie are the same. Once Bob accepts the signature, Charlie definitely accepts it. Thus, the security bound of our QDS is less than $2^{64}/(2^{128}-1) \approx 1.1 \times 10^{-19}$ for document of up to 2^{64} lengths, if one uses 128-bit key for hashing and another 256-bit key for encryption.

Secret sharing allows the key strings of Alice, Bob and Charlie to satisfy $K_a = K_b \oplus K_c$ with $K \in \{X, Y\}$,

which can be implemented with provable security by using quantum key distribution, quantum secret sharing or future quantum internet. While a full-blown quantum internet [34], with functional quantum computers and quantum repeaters as nodes connected through quantum channels, is still on the way, the first prototype of quantum internet has been realized with remote solid-state qubits [35] in multiparty entanglement applicable to secret sharing. So far, there is no workable quantum-secure asymmetric cryptosystem. With the help of secret sharing, our framework represents the first practical quantum asymmetric cryptosystem immediately applicable to secure digital signatures. Here we simulate the performances of our QDS protocol using various quantum key distribution [36–40] and quantum secret sharing [41–45] protocols (see Supplemental Material), as depicted in Fig. 2. For a gigahertz system and the symmetric channel case, the simulation results show that one can implement digital signatures up to 10^4 times per second even for 10^{10} -bit document if the fiber distance between Alice and Bob (Charlie) is 100 kilometers.

To demonstrate the full-function information security objectives, we establish a three-node quantum secure network (see Fig. 3a) containing two end nodes (Bob and Charlie) and a repeater node (Alice). Two point-to-point quantum key distribution links are built between Alice-Bob and Alice-Charlie, respectively, using the decoy-state protocol with time-bin phase encoding system [46]. Bob (Charlie) multiplexes the 1570-nm synchronization pulse with 1550-nm quantum signal by a dense wavelength division multiplexer, transmitted through a 101

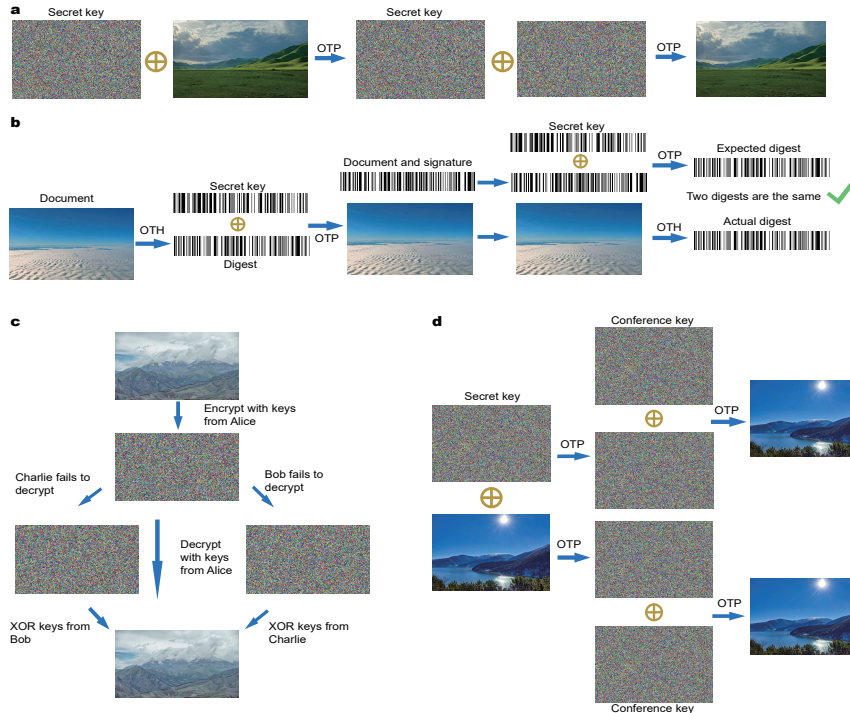


FIG. 4: **Experiment demonstration of different cryptographic tasks.** **a**, Encryption. A prairie image with 112,500 bytes is encrypted via one-time pad (OTP) to realize the perfectly private communication. The shared secret key and ciphertext are demonstrated as figures of white noise. **b**, Digital signatures. The document to be signed with the length of 130,250 bytes includes timestamp, identity number of the desert image and the image itself. The digest is composed of the hash value generated through one-time universal₂ hash functions (OTH) and the string of irreducible polynomial, and then is encrypted to form a signature by OTP. Both digest and signature are displayed as bar codes and have the same size of 32 bytes. The actual and expected digests are identical which indicates a successful digital signature. **c**, Secret sharing. An image of mountain with 79,800 bytes is used to realize provable secret sharing. The encrypted image with the same size is shown as white noise. Only when two users work together can they decrypt image. **d**, Conference key agreement. An image of lake with the size of 139,500 bytes is adopted to implement group encryption. Conference key is demonstrated as a figure of white noise. All users of this group can obtain the information of the encrypted figure separately.

km (126 km) single-mode optical fibre to Alice; the corresponding loss of quantum channels are 19 (24.3) dB and the system clock frequency is 200 MHz. To reduce insertion loss of the receiving end, we take advantage of time division multiplexing by manually switching fibre links. Classical network is used to communicate in the stage of postprocessing including parameter estimation, error correction and privacy amplification. In Fig. 3b, the blue (red) symbol refers to the experimental secret key rates between Bob-Alice (Charlie-Alice) with 6021 (470) bits per second by considering the finite-size effects, fitting well with our simulation curves. The blue and red curves are both flattened in the short distance since we introduce dead-times of 10 and 25 μ s for gated-mode InGaAs/InP single-photon detector, respectively.

In Fig. 4, we demonstrate four cryptographic tasks in our quantum secure network with information-theoretical security, including encryption, digital signatures, secret sharing and conference key agreement. Alice performs an XOR operation for her key bit strings sharing with Bob and Charlie, respectively. To realize secure encryp-

tion between Bob and Charlie, Alice announces the XOR result, as a key relay, to make Bob and Charlie share identical keys. The XOR result as the key bit string of Alice is only known by herself before the implementation of secure digital signatures and secret sharing. For conference key agreement, Alice, Bob and Charlie can obtain the same key with provable security if the XOR result of Alice is published. The demonstrated cryptographic tasks are featured by high efficiency and unconditional security on our quantum secure network using current quantum key distribution system.

In conclusion, we have successfully demonstrated a full-function quantum secure network with all information security objectives, namely, confidentiality, integrity, authenticity and non-repudiation. Particularly, we theoretically propose and experimentally implement a QDS protocol that is as practical as quantum key distribution. As such, digital signatures, which are of the central importance in internet-based digital processing systems, are now promoted to be unconditionally secure and commercially applicable by one-time pad, one-time universal₂

hashing and secret sharing. Our framework consumes few resources to sign an arbitrarily long document, surpassing all previous protocols not only in signing efficiency but also in security. The full-function quantum secure network can of course be implemented by more advanced technology, e.g., by a future quantum internet. Its successful implementation by a practical quantum secure network under current technology, as we show above, lays a firm foundation for a quantum secure layer of current internet. Such a quantum secure internet, enabling main secure cryptographic tasks simultaneously, paves the way for the quantum age of digital economy.

1. One-time pad

Define that encryption algorithm E maps plaintexts $m \in M$ to ciphertexts $c \in C$. According to Shannon's information theory, an algorithm E is perfectly secret if C and M are independent, i.e., $\Pr(m, c) = \Pr(m) \times \Pr(c)$. The one-time pad [12] encryption satisfies the above definition, where a plaintext is paired using XOR operation with a random secret key of the same length. Learning the ciphertext does not increase any information about the plaintext. Besides, each encryption requires a new and independent random key, hence, knowing details about previous key does not help the attacker. In our QDS scheme, we utilize one-time pad to encrypt the hash value and the irreducible polynomial to acquire the signature so that we can completely conceal the information of hash functions.

2. One-time LFSR-based Toeplitz hashing

A collection H of hash functions $h: \{1, \dots, M\} \rightarrow \{0, \dots, m-1\}$ is said to be universal₂ [29] if for every two different $x, y \in \{1, \dots, M\}$ we have

$$\Pr_{h \in H}[h(x) = h(y)] \leq \frac{1}{m}. \quad (1)$$

The random matrices in H are the universal₂ hash functions, which requires mn random bits for specifying hash functions (seen as an mn Boolean matrix) to transform m -bit document into n -bit hash value. To reduce the cost of random bits, Toeplitz matrix, which just requires $n+m-1$ random bits, is now widely used. Nevertheless, it still requires the length of random input bits to be longer than that of the document.

The LFSR-based Toeplitz matrix [32] is the almost universal₂ hash functions, where the hash function is determined by an irreducible polynomial $p(x)$ of degree n over Galois field $\text{GF}(2)$ and n -bit input random bits, just requiring a total of $2n$ bits. The randomness of the input string and $p(x)$ together guarantees the security of LFSR-based Toeplitz hashing and the security bound is $\epsilon = m/2^{n-1}$. In realistic setups, a crucial point is that in every round the user must randomly choose an irreducible polynomial. In our protocol, Alice finishes this task with an n -bit random number. Denote the format of the irreducible polynomial as $p(x) = x^n + a_{n-1}x^{n-1} + \dots + a_1x + a_0$, where $a_i = 0$ or 1 . Then $p(x)$ can be characterized by an n -bit string $(a_{n-1}, a_{n-2}, \dots, a_1, a_0)$, i.e., every bit of the string determines a corresponding coefficient of $p(x)$. To generate the irreducible polynomial, Alice first uses the n -bit random number to generate a polynomial $p_1(x)$, and checks out whether $p_1(x)$ is irreducible. If $p_1(x)$ is irreducible, it will be used for generating the LFSR-based Toeplitz matrix. Otherwise, Alice utilizes a new n -bit random number to get a new string and generates a new polynomial, and then examines whether it is an irreducible polynomial. Alice will repeat this step until she generates an irreducible polynomial. For example, choose $n = 128$. Assume Alice first generates $p_1(x) = x^{128} + x^{29} + x^{25} + x + 1$. Then she will find it reducible, and successively generates and examines $p_2(x) = x^{128} + x^{50} + x^{27} + x^2 + 1$, $p_3(x) = x^{128} + x^{29} + x^{27} + x^2 + 1$. Finally, she finds $p_3(x)$ irreducible and chooses $p_3(x)$ as the irreducible polynomial to generate the Toeplitz matrix. Note that for an irreducible polynomial $p(x)$, one always has $a_0 = 1$. Thus, actually we can just use $n - 1$ random bits $(a_{n-1}, a_{n-2}, \dots, a_1, 1)$ to generate the polynomial. We remark that the random number used for generating the irreducible polynomial is produced locally by Alice.

In the authentication scheme [16, 33], the input random bits can be fixed in the later rounds after the first successful round. In our QDS protocol, however, the input random bits cannot be fixed and must be randomly updated in every round. In other words, the universal₂ hash function will only be used once and then be updated. Thus, we denote it as one-time universal₂ hashing (OTH).

3. Algorithms for testing irreducibility of polynomials over $\text{GF}(2)$

The following is the concrete method we employed to check whether a polynomial over $\text{GF}(2)$ is irreducible or not.

Acknowledgments

We gratefully acknowledge support from the National Natural Science Foundation of China (No. 61801420); the Natural Science Foundation of Jiangsu Province (No. BK20211145); the Fundamental Research Funds for the Central Universities (No. 020414380182); the Key-Area Research and Development Program of Guangdong Province (No. 2020B0303040001).

Suppose $p(x)$ as a polynomial of order n in $\text{GF}(2)$. According to [30], the necessary and sufficient condition for $p(x)$ being irreducible is:

$$\begin{cases} (A) x^{2^n} \equiv x \pmod{p(x)} \\ (B) \text{gcf}\left(x^{2^{\frac{n}{d}}} - x, p(x)\right) = 1, \end{cases} \quad (2)$$

where d is any prime factor of n , $\text{gcf}(f(x), g(x))$ represents the greatest common factor (GCF) of $f(x)$ and $g(x)$. In our scheme, $n = 128 = 2^7$, i.e., n only has one prime factor “2”. Thus, to verify condition (2) we just need to examine $\text{gcf}\left(x^{2^{64}} - x, p(x)\right) = 1$.

To speed up our calculation, we utilize fast modular composition (FMC) algorithms and extended Euclidean algorithm [31]. FMC algorithms can calculate $x^{2^{128}}$ and $x^{2^{64}} \pmod{p(x)}$ with high speed by calculating $x^{2^{27}}$ and $x^{2^{26}}$, while extended Euclidean algorithm can quickly finish GCF calculation. Thus, condition (A) and (B) can be verified efficiently. In our simulation we search 1000 irreducible polynomials, and averagely it takes 73.6 tests to find an irreducible polynomial, consistent with the conclusion [32] that the total number of irreducible polynomials of order n in $\text{GF}(2)$ is at least $2^{n-1}/n$. We implement our simulation in a desktop with Intel i5-10400 CPU (with RAM of 8 GB), and averagely it takes about 0.36 seconds to generate an irreducible polynomial of order 128 from a 128-bit random input.

4. Security analysis

The key bit strings of Alice, Bob and Charlie will have the correlation of secret sharing either Alice makes an XOR operation on two strings of key obtained using quantum key distribution [36–40] or they directly carry out quantum secret sharing [41–45].

Repudiation. Successful repudiation means that Alice wishes that Bob would accept the document while Charlie rejects it. For Alice’s repudiation attacks, Bob and Charlie are both honest and symmetric and they have the same new key strings. They will make the same decision for the same document and signature. In other words, when Bob rejects (accepts) the document, Charlie also rejects (accepts) it. Therefore, our QDS protocol is immune to repudiation naturally.

Forgery. Bob forges successfully when Charlie accepts the forged document forwarded by Bob. According to our protocol, Charlie accepts the message if and only if Charlie gets the same result through one-time pad encryption and one-time universal₂ hash functions. Since the signature is encrypted by one-time pad and each hash function is utilized only one time, Bob does not have any information about the used hash function and the generated digest by Alice. Therefore, the probability of a successful forgery can be determined by

$$\epsilon_{\text{for}} = \frac{m}{2^{n-1}}, \quad (3)$$

which is the failure probability of one-time LFSR-based Toeplitz hashing, i.e., one finds two distinct documents to have the identical hash value.

5. Numerical simulation of QDS via quantum key distribution

Considering the case that we have two quantum key distribution links between Alice-Bob and Alice-Charlie, respectively, and the two links have the same loss. Alice and Bob share one set of secret key S_1 while Alice and Charlie share the other set of secret key S_2 through implementing quantum key distribution with the key rate R_{QKD} . For the requirement of secret sharing, Alice, Bob and Charlie utilize K_a , K_b and K_c as their correlation key, respectively, where $K_a = S_1 \oplus S_2$, $K_b = S_1$ and $K_c = S_2$. Therefore, the signature rate can be defined as $R_{\text{QDS}} = R_{\text{QKD}}/3n$, since one needs $3n$ -bit key to implement OTH and OTP in our QDS protocol.

(5.1) Sending-or-not-sending twin-field quantum key distribution [36].

The secure key rate is given by

$$R_{\text{QKD}} = 2t(1-t)\mu e^{-\mu} Y_1 \left[1 - H\left(e_1^{\text{ph}}\right) \right] - Q_Z f H(E^Z), \quad (4)$$

where ϵ is the probability of sending the signal pulse at a signal window, μ is the intensity of the signal pulse, Y_1 is the counting rate of Z_1 -windows, Q_Z is the observed counting rate of Z -windows, $e_1^{\text{ph}} = e_1^{X_1}$ is the phase-flip error rate for Z_1 -windows, E^Z is the bit error rate for Z -windows, and f is the error correction efficiency. The yield Y_1 and error rate $e_1^{X_1}$ can be estimated by exploiting the decoy-state method,

$$Y_1 \geq \frac{\mu/2}{\mu\nu - \nu^2} \left[e^\nu(Q_{\nu 0} + Q_{0\nu}) - \frac{\nu^2}{\mu^2} e^\mu(Q_{\mu 0} + Q_{0\mu}) - 2\frac{\mu^2 - \nu^2}{\mu^2} Q_{00} \right], \quad (5)$$

$$e_1^{X_1} \leq \frac{1}{2\nu Y_1} \left(e^{2\nu} E_{\nu\nu}^{\text{ppm}} Q_{\nu\nu}^{\text{ppm}} - \frac{1}{2} Y_0 \right), \quad (6)$$

where ν is the intensity of the decoy pulse, Q_{k_a, k_b} is the gain when Alice chooses intensity k_a and Bob chooses intensity k_b ($k_a, k_b \in \{\mu, \nu, 0\}$), $E_{\nu\nu}^{\text{ppm}}$ is the bit error rate, $Q_{\nu\nu}^{\text{ppm}}$ is the gain of intensity ν for both Alice and Bob after successful postselected phase-matching and $Y_0 = Q_{00}$ is the counting rate of vacuum state.

The gain Q_{k_a, k_b} can be given as

$$Q_{k_a, k_b} = 2(1 - p_d) e^{-\frac{k_a + k_b}{2} \sqrt{\eta}} \left[I_0 \left(\sqrt{k_a k_b} \sqrt{\eta} \right) - (1 - p_d) e^{-\frac{k_a + k_b}{2} \sqrt{\eta}} \right], \quad (7)$$

where $\eta = \eta_d^2 \times 10^{-\alpha L/10}$ is the total efficiency, η_d , α and L are the detector efficiency, attenuation coefficient and distance, respectively. p_d is the dark count rate, $I_0(x)$ is the modified Bessel function of the first kind. The gain $Q_{\nu\nu}^{\text{ppm}}$ and bit error rate $E_{\nu\nu}^{\text{ppm}}$ can be given by

$$Q_{\nu\nu}^{\text{ppm}} = Q_{c, \nu\nu}^{\text{ppm}} + Q_{e, \nu\nu}^{\text{ppm}}, \quad (8)$$

$$E_{\nu\nu}^{\text{ppm}} = [e_d^x Q_{c, \nu\nu}^{\text{ppm}} + (1 - e_d^x) Q_{e, \nu\nu}^{\text{ppm}}] / Q_{\nu\nu}^{\text{ppm}}, \quad (9)$$

where e_d^x is the misalignment rate of the X basis. Therein, the correct gain $Q_{c, \nu\nu}^{\text{ppm}}$ and incorrect gain $Q_{e, \nu\nu}^{\text{ppm}}$ are

$$Q_{c, \nu\nu}^{\text{ppm}} \approx \frac{1 - p_d}{\delta} \sqrt{\frac{\pi}{2\nu\sqrt{\eta}}} \operatorname{erf} \left(\sqrt{\frac{\nu\sqrt{\eta}}{2}} \delta \right) - (1 - p_d)^2 e^{-2\nu\sqrt{\eta}}, \quad (10)$$

$$Q_{e, \nu\nu}^{\text{ppm}} \approx \frac{1 - p_d}{\delta} e^{-2\nu\sqrt{\eta}} \sqrt{\frac{\pi}{2\nu\sqrt{\eta}}} \operatorname{erfi} \left(\sqrt{\frac{\nu\sqrt{\eta}}{2}} \delta \right) - (1 - p_d)^2 e^{-2\nu\sqrt{\eta}}, \quad (11)$$

where $\operatorname{erf}(x)$ and $\operatorname{erfi}(x)$ are the error function and imaginary error function. The gain Q_Z and bit error rate E^Z can be given by

$$Q_Z = (1 - t)^2 Q_{00} + 2t(1 - t) Q_{0\mu} + t^2 Q_{\mu\mu}, \quad (12)$$

and

$$E^Z = \frac{(1 - t)^2 Q_{00} + t^2 Q_{\mu\mu}}{(1 - t)^2 Q_{00} + t(1 - t)(Q_{0\mu} + Q_{\mu 0}) + t^2 Q_{\mu\mu}}. \quad (13)$$

In the simulation, we set $p_d = 10^{-8}$, $f = 1.1$, $\eta_d = 85\%$, $e_d = 2\%$ and $\alpha = 0.167$ dB/km. The light intensities and probability t are globally optimized.

(5.2) Phase-matching quantum key distribution [37].

Here we present the simulation details of phase-matching quantum key distribution. The overall secure key rate is given by

$$R_{\text{QKD}} = \frac{2}{D} Q_{\mu} [1 - h(E^{\text{ph}}) - fh(E^{\text{b}})], \quad (14)$$

where Q_{μ} is the total gain of the signal pulses, $2/D$ is the phase-sifting factor with $D = 16$, f is the error correction efficiency, $h(x) = -x \log_2 x - (1 - x) \log_2 (1 - x)$ is the binary entropy function, E^{ph} is the phase error rate and E^{b} is the bit error rate. The overall phase-error rate [47] is bounded by $E^{\text{ph}} \leq 1 - q_1$, where $q_1 = \mu e^{-\mu} Y_1 / Q_{\mu}$. By using the decoy state method with three intensities, the yield of single-photon component can be given as

$$Y_1 \geq \frac{\mu}{\mu\nu - \nu^2} \left(Q_{\nu} e^{\nu} - Q_{\mu} e^{\mu} \frac{\nu^2}{\mu^2} - \frac{\mu^2 - \nu^2}{\mu^2} Q_0 \right). \quad (15)$$

For simulation, the gain of intensity k ($k \in \{\mu, \nu, 0\}$) is $Q_k = 1 - (1 - 2p_d) e^{-k\eta}$. The bit error rate is $E^{\text{b}} = [p_d + \eta\mu(e_{\Delta} + e_d)] \frac{e^{-\eta\mu}}{Q_{\mu}}$, where p_d is the dark count rate, $\eta = \eta_d \times 10^{-\alpha L/20}$ is the channel transmittance, e_d is the

extra misalignment error and the intrinsic error $e_\Delta = \sin^2(\frac{\pi}{D})$. In the simulation we set $p_d = 10^{-8}$, $f = 1.1$, $\eta_d = 85\%$, $\alpha = 0.167$ dB/km and $e_d = 2\%$. The intensities μ, ν are globally optimized.

(5.3) *Discrete-modulated continuous-variable quantum key distribution [38].*

In the case of reverse reconciliation, the secret key rate under collective attacks in the asymptotic limit is given by $R_{\text{QKD}} = p_{\text{pass}}[I(X; Z) - \max_{\rho \in \mathbf{S}} \chi(Z : E)]$, where $I(X; Z)$ is the classical mutual information between Alice's string X and the raw key string Z , $\chi(Z : E)$ is the information of Eve's knowledge about the raw key string Z and $p_{\text{pass}} = 1 - \frac{1}{2} \int_{-\Delta_c}^{\Delta_c} P(q|0) dq - \frac{1}{2} \int_{-\Delta_c}^{\Delta_c} P(q|1) dq$ is the sifting probability. $P(q|0)$ and $P(q|1)$ are probability distributions of Bob's homodyne detection conditioned that Alice generates bit 0 or 1. The set \mathbf{S} contains all density operators compatible with experimental observations. According to [38], this key rate can be reformulated as a convex optimization problem and the secret key rate is $R = \min_{\rho \in \mathbf{S}} D(\mathcal{G}(\rho) || \mathcal{Z}[\mathcal{G}(\rho)]) - p_{\text{pass}} \delta_{EC}$, where $D(\rho || \sigma) = \text{Tr}(\rho \log_2 \rho) - \text{Tr}(\rho \log_2 \sigma)$ is the quantum relative entropy. \mathcal{G} is a map describing classical postprocessing. For the reverse reconciliation, we have $\mathcal{G}(\sigma) = K \sigma K^\dagger$, where $K = \sum_{z=0}^1 |z\rangle_R \otimes (|0\rangle\langle 0| + |1\rangle\langle 1|)_A \otimes (\sqrt{I_z})_B$ with $I_0 = \int_{\Delta_c}^{\infty} dq |q\rangle\langle q|$ and $I_1 = \int_{-\infty}^{-\Delta_c} dq |q\rangle\langle q|$. We set $\Delta_c = 0$ in our simulation. \mathcal{Z} is a pinching quantum channel and we have $\mathcal{Z}(\rho) = \sum_j Z_j \rho Z_j$ where $Z_0 = |0\rangle\langle 0|_R \otimes \mathcal{I}_{AB}$ and $Z_1 = |1\rangle\langle 1|_R \otimes \mathcal{I}_{AB}$. $\delta_{EC} = (1 - \beta)H(Z) + \beta h(e)$ is the amount of information leakage per signal, where $e = \frac{1}{p_{\text{pass}}} \left(\frac{1}{2} \int_{-\Delta_c}^{\Delta_c} P(q|0) dq + \frac{1}{2} \int_{\Delta_c}^{\infty} P(q|1) dq \right)$. The convex optimization problem can be described as follows

$$\begin{aligned}
& \text{minimize } D(\mathcal{G}(\rho) || \mathcal{Z}[\mathcal{G}(\rho)]) \\
& \text{subject to} \\
& \text{Tr}[\rho(|i\rangle\langle i|_A \otimes \hat{q})] = p_x \langle \hat{q} \rangle_i, \\
& \text{Tr}[\rho(|i\rangle\langle i|_A \otimes \hat{p})] = p_x \langle \hat{p} \rangle_i, \\
& \text{Tr}[\rho(|i\rangle\langle i|_A \otimes \hat{n})] = p_x \langle \hat{n} \rangle_i, \\
& \text{Tr}[\rho(|i\rangle\langle i|_A \otimes \hat{d})] = p_x \langle \hat{d} \rangle_i, \\
& \text{Tr}[\rho] = 1, \\
& \rho \geq 0, \\
& \text{Tr}_B[\rho] = \sum_{i,j=0}^3 \sqrt{p_i p_j} \langle \phi_j | \phi_i \rangle |i\rangle\langle j|_A,
\end{aligned} \tag{16}$$

where $\hat{n} = \frac{1}{2}(\hat{q}^2 + \hat{p}^2 - 1) = \hat{a}^\dagger \hat{a}$ and $\hat{d} = \hat{q}^2 - \hat{p}^2 = \hat{a}^2 + (\hat{a}^\dagger)^2$. We consider a quantum channel with transmittance $\eta = 10^{-0.167L/10}$ where L is distance and excess noise $\xi = 0.01$. In such model we have $P(q|0) = \frac{1}{\sqrt{\pi(1+\eta\xi)}} e^{-\frac{[\alpha - \sqrt{2\eta}q]^2}{1+\eta\xi}}$ and $P(q|1) = \frac{1}{\sqrt{\pi(1+\eta\xi)}} e^{-\frac{[\alpha + \sqrt{2\eta}q]^2}{1+\eta\xi}}$. The expectation values can be given by

$$\begin{aligned}
\langle \hat{q} \rangle &= \sqrt{2\eta} \text{Re}(\alpha), \\
\langle \hat{p} \rangle &= \sqrt{2\eta} \text{Im}(\alpha), \\
\langle \hat{n} \rangle &= \eta |\alpha|^2 + \frac{\eta\xi}{2}, \\
\langle \hat{d} \rangle &= \eta [\alpha^2 + (\alpha^*)^2].
\end{aligned} \tag{17}$$

α is amplitude of signal and we optimize α in the interval of [0.35, 0.6] with step of 0.01.

(5.4) *Gaussian-modulated continuous-variable quantum key distribution [39].*

From information-theoretic point of view, in the case of reverse reconciliation, Alice and Bob can distill perfectly correlated secret key bits provided that the amount of information they share I_{AB} is higher than the information acquired by Eve χ_{BE} under collective attacks. Therefore, the secret key rate is defined as $R = I_{AB} - \chi_{AB}$. Considering the inefficiency of error correction, a factor β is introduced as the reconciliation efficiency and the secret key rate formula reads $R_{\text{QKD}} = \beta I_{AB} - \chi_{AB}$. In our numerical simulation, we use $\beta = 0.95$. We calculate the mutual information using

$$I_{AB} = \frac{1}{2} \log_2 \frac{V + \chi_{\text{tot}}}{1 + \chi_{\text{tot}}}, \tag{18}$$

where V is the variance of the thermal state observed at Alice's lab, and χ_{tot} is the total excess noise added between Alice and Bob. Here we detail the formula of χ_{tot} as follows

$$\chi_{tot} = \frac{1}{\eta T(1 + v_{el}) + \xi - 1}, \quad (19)$$

where T is the transmission of quantum channel, ξ is the excess noise, v_{el} is electronic noise and η is detection losses. To draw the line, we set $\eta = 0.85$, $v_{el} = 0$, $\xi = 0.01$, $T = 10^{-0.167L/10}$ and V is optimized. L is the distance. Under collective attacks, Eve's accessible information is upper bounded by the Holevo quantity χ_{BE} satisfying

$$\chi_{BE} = G\left(\frac{\lambda_1 - 1}{2}\right) + G\left(\frac{\lambda_2 - 1}{2}\right) - G\left(\frac{\lambda_3 - 1}{2}\right) - G\left(\frac{\lambda_4 - 1}{2}\right), \quad (20)$$

where $G(x) = (x+1)\log_2(x+1) - x\log_2 x$, and $\{\lambda_i\}$ are the symplectic eigenvalues of the covariance matrix characterizing the quantum state. Calculation shows that $\lambda_{1,2}^2 = \frac{1}{2}[A \pm \sqrt{A^2 - 4B}]$, where $A = V^2(1-2T) + 2T + T^2(V + \xi - 1 + \frac{1}{T})^2$ and $B = T^2(V/T - V + V\xi + 1)^2$ and $\lambda_{3,4}^2 = \frac{1}{2}[C \pm \sqrt{C^2 - 4D}]$, where $C = \frac{V\sqrt{B} + T(V + 1/T - 1 + \xi) + A/\eta(1 + v_{el}) - A}{T(V + \chi_{tot})}$ and $D = \sqrt{B} \frac{V + \sqrt{B}[1/\eta(1 + v_{el}) - 1]}{T(V + \chi_{tot})}$.

(5.5) Measurement-device-independent quantum key distribution [40].

For measurement-device-independent quantum key distribution, we consider Alice and Bob sending coherent state and the ideal case where only the channel loss and detector efficiency are taken into consideration. The secret key rate is given by

$$R_{\text{QKD}} = \frac{1}{2e^2} \eta^2, \quad (21)$$

where $\eta = \eta_d \times 10^{-\alpha L/20}$ is the total channel transmittance, L is the distance between Alice and Bob. We set $\eta_d = 85\%$, $\alpha = 0.167$ dB/km.

6. Numerical simulation of QDS via quantum secret sharing

Different from quantum key distribution, quantum secret sharing can directly offer the secret sharing correlation with unconditional security via quantum laws. In quantum secret sharing of three users, Alice is the dealer while both Bob and Charlie are players. Even though one of Bob and Charlie is dishonest, they can also generate the secure correlation key $K_a = K_b \oplus K_c$. We assume that the distance of Alice-Bob and Alice-Charlie are the same. The signature rate can be defined as $R_{\text{QDS}} = R_{\text{QSS}}/3n$, since one needs $3n$ -bit key for OTH and OTP.

(6.1) Prepare-and-measure quantum secret sharing [41].

Using Greenberger-Horne-Zeilinger (GHZ) state can realize quantum secret sharing directly. Here, we consider an equivalent prepare-and-measure protocol. In our simulation, we only consider the photon loss in quantum channel and detector. Therefore, the secret key rate is given by

$$R_{\text{QSS}} = \eta^2, \quad (22)$$

where $\eta = \eta_d \times 10^{-\alpha L/10}$, $\eta_d = 85\%$ and $\alpha = 0.167$ dB/km. L is the distance between Alice and Bob (Charlie).

(6.2) Measurement-device-independent quantum secret sharing [42].

By exploiting the postselected GHZ state, one can also realize quantum secret sharing. We only consider the photon loss from quantum channels and detectors here. The secret key rate of using single-photon source can be given by

$$R_{\text{QSS}} = \frac{1}{4} \eta_d \eta^2. \quad (23)$$

Here we have $\eta = \eta_d \times 10^{-\alpha L/10}$, $\eta_d = 85\%$, $\alpha = 0.167$ dB/km and assume that there is no loss of Alice's photon. The factor $1/4$ comes from that only two of eight GHZ states can be identified. L is the distance between Alice and Bob (Charlie).

(6.3) Round-robin quantum secret sharing [43]. The secret key rate per pulse of the round-robin quantum secret sharing with twin-field for sending d coherent pulses each train in the case of the inside adversary can be written as

$$R_{\text{QSS}} = \frac{1}{d} \{ \hat{Q}[1 - h(\hat{e}_p)] - Qfh(e_b) \}, \quad (24)$$

TABLE I: List of the experimental data using for one-time secure key generation.

	Alice-Bob (101 km)	Alice-Charlie (126 km)
n_μ^z	4616266	5225387
n_ν^z	258671	296285
n_ω^z	394425	437496
n_0^z	11189	14080
n_μ^x	1035046	1311484
n_ν^x	58107	78890
n_ω^x	87317	110362
n_0^x	3126	8168
m_ω^z	3446	9401

where we have $\hat{Q} = \min\{Q_A, Q_B\}$. Q_A and Q_B are gains of Charlie's successful detection from Alice and Bob, respectively. The phase error rate is

$$\hat{e}_p = \frac{\epsilon_{\text{src}}}{\hat{Q}} + \left(1 - \frac{\epsilon_{\text{src}}}{\hat{Q}}\right) \frac{n_{\text{th}}}{d-1}. \quad (25)$$

The average gain Q and bit error rate e_b of each train can be written as

$$Q = \frac{1}{2}[1 - (1 - dp_d)e^{-2\mu\eta}], \quad (26)$$

and

$$e_b = \frac{e_d(1 - e^{-2\mu\eta}) + dp_de^{-2\mu\eta}/2}{1 - (1 - dp_d)e^{-2\mu\eta}}, \quad (27)$$

where $\eta = \eta_d \times 10^{-\alpha L/10}$ is the efficiency between Alice and Bob (Charlie). Besides, we have the gains $Q_A = Q_B = Q/2$ due to the symmetry. Let n be the total photon number in a train of optical pulses with total intensity μ . Then, the probability of finding more than n_{th} photons in a train of optical pulses can be written as

$$\Pr(n > n_{\text{th}}) = e_{\text{src}} := 1 - \sum_{n=0}^{n_{\text{th}}} \frac{e^{-\mu} \mu^n}{n!}, \quad (28)$$

where n_{th} is an integer constant chosen in this protocol. For simulation we set $p_d = 10^{-8}$, $f = 1.1$, $\eta_d = 85\%$, $\alpha = 0.167$ dB/km and $e_d = 2\%$. The intensity μ , the selected integer n_{th} and the number of optical pulses d are globally optimized.

(6.4) Single-qubit quantum secret sharing [44].

For the single-qubit quantum secret sharing protocol with single photon source, the final key rate can be easily derived based on phase-error correction

$$R_{\text{QSS}} = Q_1[1 - h(e_p) - fh(e_b)], \quad (29)$$

where $e_p = e_b = p_d(1 - 2e_d)/Q_1 + e_d$ and $Q_1 = \mu e^{-\mu}(2p_d + \eta - 2p_d\eta)$. $\eta = \eta_d \times 10^{-\alpha \cdot 2L/10}$ is the total transmittance; $2L$ is the total distance. The intensity μ is globally optimized. We set $p_d = 10^{-8}$, $f = 1.1$, $\eta_d = 85\%$, $\alpha = 0.167$ dB/km and $e_d = 2\%$.

(6.5) Differential-phase-shift quantum secret sharing [45].

The final key rate for differential-phase-shift quantum secret sharing using twin-field is bounded by

$$R_{\text{QSS}} = Q_\mu[-(1 - 2\mu) \log_2(P_{\text{co}}) - fh(E_\mu)], \quad (30)$$

where Q_μ is the gain of the whole system. $h(x) = -x \log_2(x) - (1-x) \log_2(1-x)$ is Shannon entropy and f is the error correction efficiency. P_{co} is the upper bound of collision probability when considering individual attacks, which

TABLE II: List of the calculation results using for one-time secure key generation.

	Alice-Bob (101 km)	Alice-Charlie (126 km)
R_{QKD} (bps)	6021	470
Λ (s)	152.8	561
s_0^{zz}	159429	203152
s_1^{zz}	2756924	3158726
λ_{EC}	1225992	1659948
ℓ	920042	263482
$\overline{\phi}_1^{zz}$	4.83%	9.57%
ε_{sec}	10^{-10}	10^{-10}

can be concluded as $P_{\text{co}} = 1 - E_\mu^2 - (1 - 6E_\mu)^2/2$. The total gain and the total error rate with an intensity of μ is given by

$$\begin{aligned} Q_\mu &= 1 - (1 - 2p_d)e^{-\mu\eta}, \\ E_\mu Q_\mu &= e_d Q_\mu + \left(\frac{1}{2} - e_d\right) 2p_d e^{-\mu\eta}, \end{aligned} \quad (31)$$

where e_d is the misalignment error rate of detectors. The $\eta = \eta_d \times 10^{-\alpha L/10}$ is the efficiency between Alice and Bob (Charlie), where η_d is detection efficiency of Charlie's detectors. The intensity is globally optimized. We set $p_d = 10^{-8}$, $f = 1.16$, $\eta_d = 85\%$, $\alpha = 0.167$ dB/km and $e_d = 2\%$.

7. Experimental details

In the transmitting end, a master laser generates a repetition rate of 200 MHz and phase-randomized laser pulses with 1.6 ns-wide at 1550.12 nm. An asymmetric interferometer with 2 ns time delay divides each master pulse into two pairs of optical pulses with relative phases 0 and π . Then, the two pair optical pulses are injected into two slave lasers through the optical circulator, respectively. With the help of controlling the trigger electrical signal of two slave lasers, one generates quantum signal only in the first time-bin or the second time-bin to constitute the Z basis, and one prepares quantum signal both in two time-bins with 0 or π phase difference to constitute the X basis. A 50 GHz bandwidth fibre Bragg grating is exploited to pre-compensate for the pulse broadening and to remove extra spurious emission. The 2 ns-wide synchronization pulses with repetition rates of 100 kHz are transmitted via the quantum channel by using wavelength division multiplexed. The slave pulse width is 400 ps which is much larger than the 10 ps timing resolution of programmable delay chip, which means that time consistency can be accurately calibrated. The spectral consistency is naturally satisfied through the laser seeding technique [48].

In the receiving end, a 30:70 biased beam splitter is used to perform passive basis detection after a wavelength division demultiplexer. A probability of 30% is measured in phase interference and the probability of 70% is used to receive in the time basis. A Faraday-Michelson interferometer realizes the phase measurement, where phase drift is compensated in real time by using the phase shifter. The total insertion loss of the time and phase bases are 4.25 and 8 dB, respectively. The efficiency of single-photon detectors is 20% at a 160 dark count per second. To decrease the after-pulse probability, we set the dead times to be 10 and 25 μs for Bob-Alice and Charlie-Alice links, respectively.

A four-intensity decoy-state protocol [49–51] is adopted, where the intensities of the Z basis are set as $\mu = 0.35$ and $\nu = 0.15$, the intensity of the X basis is $\omega = 0.3$. The intensity of vacuum state is 0, which does not contain any basis information. The corresponding probabilities are $p_\mu = 0.78$, $p_\nu = 0.1$, $p_\omega = 0.08$ and $p_0 = 0.04$. Thereinto, the amplitude modulator generates two different intensities and the intensity of ω is double of ν since it has two pulses in the X basis.

The error correction and privacy amplification are carried out using a field-programmable gate array. Each time privacy amplification will be performed after accumulating data approximately to the size of 4 Mb via about ten times of error correction, where the data size excludes the amount of information leaked in error correction. For the link of Alice-Bob with 101 km (Alice-Charlie with 126 km), one needs to accumulate about 153 (560) seconds of data for privacy amplification to extract secure key. Here we only list the experimental data of one set and calculation results related to privacy amplification, as shown in Tables I and II.

In order to compare with the experimental results, we use the relevant experimental parameters to simulate the secure key rate, as shown in Table III. The length of final key which is ε_{cor} -correct and ε_{sec} -secret can be given by [46, 52]

$$\ell = s_0^{zz} + s_1^{zz} \left[1 - h\left(\overline{\phi}_1^{zz}\right) \right] - \lambda_{\text{EC}} - \log_2 \frac{2}{\varepsilon_{\text{cor}}} - 6 \log_2 \frac{22}{\varepsilon_{\text{sec}}}, \quad (32)$$

TABLE III: Simulation parameters of the link between Alice-Bob (Charlie). e_d^z and e_d^x are the misalignment rate of the Z and X bases and t_{dead} is the dead time of detector.

Clock frequency	η_d	p_d	e_d^z	e_d^x	t_{dead}	ε_{cor}	f
2×10^8	20%	0.8×10^{-6}	2.3% (2.2%)	1.9% (2.4%)	10 (25) μs	10^{-15}	1.42

where $h(x) := -x \log_2 x - (1-x) \log_2(1-x)$. Thereinto, \bar{x} (\underline{x}) denotes the upper (lower) bound of observed value x . Using the decoy-state method for finite sample sizes, the expected numbers of vacuum event $\underline{s}_0^{zz^*}$ and single-photon event $\underline{s}_1^{zz^*}$ can be written as

$$\underline{s}_0^{zz^*} \geq (e^{-\mu} p_\mu + e^{-\nu} p_\nu) \frac{n_0^{zz^*}}{p_0}, \quad (33)$$

and

$$\underline{s}_1^{zz^*} \geq \frac{\mu^2 e^{-\mu} p_\mu + \mu \nu e^{-\nu} p_\nu}{\mu \nu - \nu^2} \times \left(e^\nu \frac{n_\nu^{zz^*}}{p_\nu} - \frac{\nu^2}{\mu^2} e^\mu \frac{\bar{n}_\mu^{zz^*}}{p_\mu} - \frac{\mu^2 - \nu^2}{\mu^2} \frac{\bar{n}_0^{zz^*}}{p_0} \right), \quad (34)$$

where $n_k^{z(x)}$ is the count of k ($k \in \{\mu, \nu, \omega\}$) intensity pulse measured in the $Z(X)$ basis, x^* is the corresponding expected value of given observed value x . The upper and lower bound can be acquired [53] by using the variant of the Chernoff bound, $\bar{x}^* = x + \beta + \sqrt{2\beta x + \beta^2}$ and $\underline{x}^* = x - \frac{\beta}{2} - \sqrt{2\beta x + \frac{\beta^2}{4}}$, where $\beta = \ln \frac{22}{\varepsilon_{\text{sec}}}$. The expected number of single-photon event $\underline{s}_1^{xx^*}$ in \mathcal{X}_ω can be given by [51]

$$\underline{s}_1^{xx^*} \geq \frac{\mu \omega e^{-\omega} p_\omega}{\mu \nu - \nu^2} \left(e^\nu \frac{n_\nu^{xx^*}}{p_\nu} - \frac{\nu^2}{\mu^2} e^\mu \frac{\bar{n}_\mu^{xx^*}}{p_\mu} - \frac{\mu^2 - \nu^2}{\mu^2} \frac{\bar{n}_0^{xx^*}}{p_0} \right). \quad (35)$$

Besides, the expected number of bit error $\bar{t}_1^{xx^*}$ associated with the single-photon event in \mathcal{X}_ω is $\bar{t}_1^{xx^*} \leq m_\omega^x - \underline{t}_0^{xx^*}$, with $\underline{t}_0^{xx^*} = \frac{e^{-\omega} p_\omega}{2p_0} n_0^{xx^*}$. For a given expected value, the upper and lower bounds of observed value can be given as $\bar{x} = x^* + \frac{\beta}{2} + \sqrt{2\beta x^* + \frac{\beta^2}{4}}$ and $\underline{x} = x^* - \sqrt{2\beta x^*}$. By using the random sampling without replacement, the phase error rate in the Z basis is

$$\bar{\phi}_1^{zz} = \frac{\bar{t}_1^{xx^*}}{\underline{s}_1^{xx^*}} + \gamma^U \left(\underline{s}_1^{zz}, \underline{s}_1^{xx^*}, \frac{\bar{t}_1^{xx^*}}{\underline{s}_1^{xx^*}}, \frac{\varepsilon_{\text{sec}}}{22} \right), \quad (36)$$

where we have $\gamma^U(n, k, \lambda, \epsilon) = \frac{\frac{(1-2\lambda)AG}{n+k} + \sqrt{\frac{A^2 G^2}{(n+k)^2} + 4\lambda(1-\lambda)G}}{2 + 2\frac{A^2 G}{(n+k)^2}}$, with $A = \max\{n, k\}$ and $G = \frac{n+k}{nk} \ln \frac{n+k}{2\pi nk \lambda (1-\lambda) \epsilon^2}$.

-
- [1] A. Fedorov, E. Kiktenko, and A. Lvovsky, *Nature* **563**, 465 (2018).
 - [2] A. J. Menezes, P. C. Van Oorschot, and S. A. Vanstone, *Handbook of applied cryptography* (CRC press, 2018).
 - [3] X. Wang and H. Yu, in *Advances in Cryptology-Eurocrypt 05* (Springer, 2005), vol. 3494 of *LNCS*.
 - [4] X. Wang, Y. L. Yin, and H. Yu, in *Advances in Cryptology - CRYPTO 2005: 25th Annual International Cryptology Conference, Santa Barbara, California, USA, August 14-18, 2005, Proceedings* (2005), vol. 3621 of *Lecture Notes in Computer Science*.
 - [5] M. Stevens, E. Bursztein, P. Karpman, A. Albertini, and Y. Markov, in *Advances in Cryptology - CRYPTO 2017* (Springer, 2017), vol. 10401 of *LNCS*, pp. 570–596.
 - [6] T. Kleinjung, K. Aoki, J. Franke, A. K. Lenstra, E. Thomé, J. W. Bos, P. Gaudry, A. Kruppa, P. L. Montgomery, D. A. Osvik, et al., in *Advances in Cryptology - CRYPTO 2010* (2010).
 - [7] T. Kleinjung, C. Diem, A. K. Lenstra, C. Priplata, and C. Stahlke, in *Annual International Conference on the Theory and Applications of Cryptographic Techniques* (Springer, 2017), pp. 185–201.
 - [8] F. Boudot, P. Gaudry, A. Guillevic, N. Heninger, E. Thomé, and P. Zimmermann, in *Annual International Cryptology Conference* (Springer, 2020), pp. 62–91.
 - [9] R. L. Rivest, A. Shamir, and L. Adleman, *Commun. ACM* **21** (1978).
 - [10] T. Elgamal, *IEEE Transactions on Information Theory* **31**, 469 (1985).
 - [11] P. W. Shor, in *Proceedings 35th annual symposium on foundations of computer science* (IEEE, 1994), pp. 124–134.

- [12] C. E. Shannon, *The Bell System Technical Journal* **27**, 379 (1948).
- [13] C. H. Bennett and G. Brassard, *Theor. Comput. Sci.* **560**, 7 (2014).
- [14] B. Fröhlich, J. F. Dynes, M. Lucamarini, A. W. Sharpe, Z. Yuan, and A. J. Shields, *Nature* **501**, 69 (2013).
- [15] S. Wengerowsky, S. K. Joshi, F. Steinlechner, H. Hübel, and R. Ursin, *Nature* **564**, 225 (2018).
- [16] Y.-A. Chen, Q. Zhang, T.-Y. Chen, W.-Q. Cai, S.-K. Liao, J. Zhang, K. Chen, J. Yin, J.-G. Ren, Z. Chen, et al., *Nature* **589**, 214 (2021).
- [17] D. Gottesman and I. Chuang, arXiv preprint quant-ph/0105032 (2001).
- [18] P. J. Clarke, R. J. Collins, V. Dunjko, E. Andersson, J. Jeffers, and G. S. Buller, *Nature Commun.* **3**, 1174 (2012).
- [19] V. Dunjko, P. Wallden, and E. Andersson, *Phys. Rev. Lett.* **112**, 040502 (2014).
- [20] H.-L. Yin, Y. Fu, and Z.-B. Chen, *Phys. Rev. A* **93**, 032316 (2016).
- [21] R. Amiri, P. Wallden, A. Kent, and E. Andersson, *Phys. Rev. A* **93**, 032325 (2016).
- [22] Y.-S. Lu, X.-Y. Cao, C.-X. Weng, J. Gu, Y.-M. Xie, M.-G. Zhou, H.-L. Yin, and Z.-B. Chen, *Opt. Express* **29**, 10162 (2021).
- [23] R. J. Collins, R. J. Donaldson, V. Dunjko, P. Wallden, P. J. Clarke, E. Andersson, J. Jeffers, and G. S. Buller, *Phys. Rev. Lett.* **113**, 040502 (2014).
- [24] H.-L. Yin, Y. Fu, H. Liu, Q.-J. Tang, J. Wang, L.-X. You, W.-J. Zhang, S.-J. Chen, Z. Wang, Q. Zhang, et al., *Phys. Rev. A* **95**, 032334 (2017).
- [25] H.-L. Yin, W.-L. Wang, Y.-L. Tang, Q. Zhao, H. Liu, X.-X. Sun, W.-J. Zhang, H. Li, I. V. Puthoor, L.-X. You, et al., *Phys. Rev. A* **95**, 042338 (2017).
- [26] G. Roberts, M. Lucamarini, Z. Yuan, J. Dynes, L. Comandar, A. Sharpe, A. Shields, M. Curty, I. Puthoor, and E. Andersson, *Nature Commun.* **8**, 1098 (2017).
- [27] X.-B. An, H. Zhang, C.-M. Zhang, W. Chen, S. Wang, Z.-Q. Yin, Q. Wang, D.-Y. He, P.-L. Hao, S.-F. Liu, et al., *Opt. Lett.* **44**, 139 (2019).
- [28] S. Richter, M. Thornton, I. Khan, H. Scott, K. Jaksch, U. Vogl, B. Stiller, G. Leuchs, C. Marquardt, and N. Korolkova, *Phys. Rev. X* **11**, 011038 (2021).
- [29] J. L. Carter and M. N. Wegman, *Journal of Computer and System Sciences* **18**, 143 (1979).
- [30] M. O. Rabin, *SIAM Journal on computing* **9**, 273 (1980).
- [31] J. Von Zur Gathen and J. Gerhard, *Modern computer algebra* (Cambridge university press, 2013).
- [32] H. Krawczyk, in *Annual International Cryptology Conference* (1994), pp. 129–139.
- [33] C.-H. F. Fung, X. Ma, and H. Chau, *Phys. Rev. A* **81**, 012318 (2010).
- [34] S. Wehner, D. Elkouss, and R. Hanson, *Science* **362** (2018).
- [35] M. Pompili, S. L. N. Hermans, S. Baier, H. K. C. Beukers, P. C. Humphreys, R. N. Schouten, R. F. L. Vermeulen, M. J. Tiggeleman, L. dos Santos Martins, B. Dirkse, et al., *Science* **372**, 259 (2021).
- [36] X.-B. Wang, Z.-W. Yu, and X.-L. Hu, *Phys. Rev. A* **98**, 062323 (2018).
- [37] X. Ma, P. Zeng, and H. Zhou, *Phys. Rev. X* **8**, 031043 (2018).
- [38] J. Lin, T. Upadhyaya, and N. Lütkenhaus, *Phys. Rev. X* **9**, 041064 (2019).
- [39] J. Lodewyck, M. Bloch, R. García-Patrón, S. Fossier, E. Karpov, E. Diamanti, T. Debuisschert, N. J. Cerf, R. Tualle-Brouri, S. W. McLaughlin, et al., *Phys. Rev. A* **76**, 042305 (2007).
- [40] H.-K. Lo, M. Curty, and B. Qi, *Phys. Rev. Lett.* **108**, 130503 (2012).
- [41] M. Hillery, V. Bužek, and A. Berthiaume, *Phys. Rev. A* **59**, 1829 (1999).
- [42] Y. Fu, H.-L. Yin, T.-Y. Chen, and Z.-B. Chen, *Phys. Rev. Lett.* **114**, 090501 (2015).
- [43] J. Gu, Y.-M. Xie, W.-B. Liu, Y. Fu, H.-L. Yin, and Z.-B. Chen, *Opt. Express* **29**, 32244 (2021).
- [44] C. Schmid, P. Trojek, M. Bourennane, C. Kurtsiefer, M. Żukowski, and H. Weinfurter, *Phys. Rev. Lett.* **95**, 230505 (2005).
- [45] J. Gu, X.-Y. Cao, H.-L. Yin, and Z.-B. Chen, *Opt. Express* **29**, 9165 (2021).
- [46] H.-L. Yin, P. Liu, W.-W. Dai, Z.-H. Ci, J. Gu, T. Gao, Q.-W. Wang, and Z.-Y. Shen, *Opt. Express* **28**, 29479 (2020).
- [47] P. Zeng, W. Wu, and X. Ma, *Phys. Rev. Appl.* **13**, 064013 (2020).
- [48] L. Comandar, M. Lucamarini, B. Fröhlich, J. Dynes, A. Sharpe, S.-B. Tam, Z. Yuan, R. Penty, and A. Shields, *Nat. Photonics* **10**, 312 (2016).
- [49] X.-B. Wang, *Phys. Rev. Lett.* **94**, 230503 (2005).
- [50] H.-K. Lo, X. Ma, and K. Chen, *Phys. Rev. Lett.* **94**, 230504 (2005).
- [51] Z.-W. Yu, Y.-H. Zhou, and X.-B. Wang, *Phys. Rev. A* **93**, 032307 (2016).
- [52] C. C. W. Lim, M. Curty, N. Walenta, F. Xu, and H. Zbinden, *Phys. Rev. A* **89**, 022307 (2014).
- [53] H.-L. Yin, M.-G. Zhou, J. Gu, Y.-M. Xie, Y.-S. Lu, and Z.-B. Chen, *Sci. Rep.* **10**, 14312 (2020).